POLITECNICO DI TORINO
Repository ISTITUZIONALE

3D self-organized microvascular model of the human blood-brain barrier with endothelial cells, pericytes and astrocytes

Original
3D self-organized microvascular model of the human blood-brain barrier with endothelial cells, pericytes and astrocytes / Campisi, M., Shin, Y., Osaki, T., Hajal, C., Chiono, V., Kamm, R.D.. - In: BIOMATERIALS. - ISSN 0142-9612. - ELETTRONICO. - 180:(2018), pp. 117-129. [10.1016/j.biomaterials.2018.07.014]

Availability:
This version is available at: 11583/2716982 since: 2018-11-10T16:56:49Z

Publisher:
Elsevier Ltd

Published
DOI:10.1016/j.biomaterials.2018.07.014

Terms of use:

This article is made available under terms and conditions as specified in the corresponding bibliographic description in the repository

Publisher copyright
Elsevier postprint/Author's Accepted Manuscript

© 2018. This manuscript version is made available under the CC-BY-NC-ND 4.0 license
http://creativecommons.org/licenses/by-nc-nd/4.0/.The final authenticated version is available online at:
http://dx.doi.org/10.1016/j.biomaterials.2018.07.014

(Article begins on next page)

07 October 2026

3D Self-Organized Microvascular Model of the Human Blood-Brain Barrier with Endothelial Cells, Pericytes and Astrocytes

Marco Campisi[1,2], Yoojin Shin[2], Tatsuya Osaki[2], Cynthia Hajal[2], Valeria Chiono[1], Roger D. Kamm[2,3,4] *

[1] Department of Mechanical and Aerospace Engineering, Politecnico di Torino, Corso Duca degli Abruzzi 24, 10129 Turin, Italy.

[2] Department of Mechanical Engineering, Massachusetts Institute of Technology, 500 Technology Square, MIT Building, Room NE47-321, Cambridge, MA, 02139, United States of America.

[3] Department of Biological Engineering, Massachusetts Institute of Technology, 500 Technology Square, MIT Building, Room NE47-321, Cambridge, MA, 02139, United States of America.

[4] Singapore-MIT Alliance for Research&Technology (SMART), BioSytems and Micromechanics (BioSym), Singapore, Singapore.

*Corresponding author: Roger D. Kamm: rdkamm@mit.edu

Keywords: Human Blood-Brain Barrier; *In Vitro* Modeling; Microfluidic Device; Self-Assembled Microvascular Network; Induced Pluripotent Stem Cell-Derived Endothelial Cells; Drug Delivery Test Platform.

Abstract

The blood-brain barrier (BBB) regulates molecular trafficking, protects against pathogens, and prevents efficient drug delivery to the brain. Models to date failed to reproduce the human anatomical complexity of brain barriers, contributing to misleading results in clinical trials. To overcome these limitations, a novel 3-dimensional BBB microvascular network model was developed via vasculogenesis to accurately replicate the *in vivo* neurovascular organization. This microfluidic system includes human induced pluripotent stem cell-derived endothelial cells, brain pericytes, and astrocytes as self-assembled vascular networks in fibrin gel. Gene expression of membrane transporters, tight junction and extracellular matrix proteins, was consistent with computational analysis of geometrical structures and quantitative immunocytochemistry, indicating BBB maturation and microenvironment remodeling. Confocal microscopy validated microvessel-pericyte/astrocyte dynamic contact-interactions. The BBB model exhibited perfusable and selective microvasculature,

with permeability lower than conventional *in vitro* models, and similar to *in vivo* measurements in rat brain. This robust and physiologically relevant BBB microvascular model offers an innovative and valuable platform for drug discovery to predict neuro-therapeutic transport efficacy in pre-clinical applications as well as recapitulate patient-specific and pathological neurovascular functions in neurodegenerative disease.

Introduction

The blood-brain barrier (BBB) and blood-spinal cord barrier help maintain brain homeostasis [1] by regulating the transport of necessary nutrients, ions, and hormones, while preventing the entry of neurotoxins or pathogens into the brain owing to a complex membrane transport mechanism [2]. The BBB consists of specialized endothelial cells (ECs) interconnected by junctional complexes including tight junctions (TJs) and adherens junctions, surrounded by pericytes (PCs) and astrocytes (ACs), and ensheathed in a basal lamina. Each of these specialized features contributes to BBB integrity, and to the control of transport processes [3]. Loss of BBB integrity is associated with Alzheimer's disease [4][5], Parkinson's disease [6], and multiple sclerosis [7], as well as with brain cancer [8]. Furthermore, the BBB regulates active and passive transport of solutes into the brain [9][10], posing an obstacle to drug delivery for the treatment of neurological diseases and brain tumors [11][12].

For these reasons, preclinical models of the BBB are developed to understand its role in the pathogenesis of neurological diseases as well as to evaluate drug permeability. For years, *in vivo* animal models have been used to model the BBB and study drug delivery [13]. Although these techniques are considered the gold standard, 80% of successful drug candidates in animal models later failed in clinical trials [14][15].

To optimize the design of innovative therapies and drug carriers, a robust, reliable, and cost-effective *in vitro* BBB model that adequately reflects human *in vivo* conditions is required [16][17]. For several decades, transwell assays have been widely adopted to assess drug permeability by culturing a confluent monolayer of ECs in the absence or presence of PCs or ACs [18]. Although this system is reproducible and easy to use, it has limitations in mimicking fundamental BBB features and microenvironmental complexities such as cell-cell or cell-matrix interactions, compromising its ability to accurately model brain capillaries in terms of junctional proteins and membrane transporter

expression [17][19][20]. Recently, BBB spheroids have been developed to study organogenesis and the transport of brain penetrating agents [21][22]. Although these systems are cost-effective, they are limited in their ability to recreate a realistic and relevant BBB morphology. As an alternative to simple culture models, microfluidic technology offers a promising tool for reconstituting the BBB with several advantages: microfluidic systems allow for precise control of the 3D cellular and extracellular matrix (ECM) microenvironment, while providing a platform for the study of cellular and structural responses to various stimuli. These systems mimic the complex cellular interactions and structures found in many tissues or organs *in vivo*, and are thus referred to as 'organ-on-a-chip' [23][24]. Recently, efforts to reconstitute a 3D BBB model within a microfluidic system have accelerated with the development of organ-on-a-chip assays to study immune cell transmigration [25], metastatic cancer extravasation to the brain [26], as well as vessel formation in a tubular shape [27]. However, systems to date have relatively large diameters (~ 600-800 µm) [27] compared to the dimension of human BBB vasculature *in vivo* (arterioles and venules 10-100 µm; capillaries 7-10 µm) [28][29], and fail to recapitulate BBB microvasculature morphology and development in terms of mature cell-cell interactions via natural biological processes, as well as physiological blood flow rates and wall shear stresses needed to activate mechanosensing/mechanotransduction pathways, thus altering realistic transport exchange mechanisms at the level of brain capillaries [30][31].

Two microfluidic models have been recently reported using a co-culture of human ECs and rat neurons and ACs. One incorporated a compartmentalized 3D monolayer of human cerebral microvascular ECs in co-culture with primary rat ACs and neurons [32]. In a separate study, similar to the previous model [33], a BBB microvascular network (µVN) platform created by a vasculogenesis-like process, culturing human umbilical vein endothelial cells (HUVECs) in a 3D ECM-mimetic hydrogel showed that direct interaction with neural tissue from the rat cortex was responsible for the low permeability values measured [34].

However, while co-cultures with cells from different species are advantageous in terms of accessibility and ease of genetic manipulations, cross-species compatibility remains a concern regarding the relevance of these results to human physiology [35]. Moreover, HUVECs offer a poor model for cerebral vasculature, while PCs, recognized to be a key component of the BBB [35], have not been considered in these models [32][34].

To address the main limitations of the current state-of-the-art models, we reasoned that a BBB model developed from human cells co-cultured in a 3D microenvironment would better replicate the human BBB, based on the hypothesis that the co-culture arrangement could support the maturation and differentiation of human iPS cell-derived endothelial cells (iPSC-ECs) into BBB microvascular cells. Hence, a 3D BBB microfluidic model was designed consisting of self-assembled μVNs from human iPSC-ECs as well as human primary brain PCs, and human primary ACs, where all cell types spontaneously assembled into a modular organization reproducing the BBB structure being in dynamic and direct contact with each other.

BBB functionality was evaluated by progressive increase of co-culture complexity up to a tri-culture of iPSC-ECs, PCs, and ACs. Confocal imaging and immunocytochemistry, permeability measurements and gene expression analysis were used to quantitatively assess BBB characteristics. Such human 3D BBB model has unique biological features, representing a promising platform for *in vitro* preclinical experimentation.

Materials and methods

Fabrication of the microfluidic device (micro-device/macro-device)

The 3D microfluidic systems were composed of polydimethylsiloxane (PDMS; Sylgard 184; Dow Corning, MI, USA) with a single layer microchannel and two fluid channels, fabricated by soft lithography [36] (Fig. 1c, Supplementary Fig. 1a-b). Elastomer and curing agent were mixed (10:1 volume ratio), degassed and poured onto a silicon master and cured overnight at 60°C. I/O holes were created with biopsy punches, then the device was taped to remove dust and sterilized as previously described [37]. The PDMS micro and macro-devices were treated with oxygen plasma (Harrick Plasma), then bonded to a glass coverslip (Fisher Scientific) coated with poly(D-lysine hydrobromide) (PDL, Sigma-Aldrich) solution (1 mg/ml) and, finally, placed in an incubator for 3 h at 37°C, rinsed 3 times and dried overnight.

Cell culture and device seeding of BBB self-assembled vascular network model

Human iPSC-ECs (Cellular Dynamics International, CDI) were subcultured on flasks coated with human fibronectin (30 µg/ml, Millipore) in vascular medium (VascuLife VEGF Medium Complete Kit, icell media supplement, CDI). Pericytes and astrocytes isolated from human brain (ScienCell), were cultured in growth medium (ScienCell) on a poly-l-lysine (Sigma-Aldrich) coated flask, and maintained in a humidified incubator (37 °C, 5% CO2), replacing the medium every 2 days. Cells were detached using TrypLE (for iPSC-ECs) and 0.025% trypsin/EDTA for other cell types (Thermo Fisher). Experiments were performed between passages 3 and 5 for all cells.

Fibrinogen (6 mg/ml) and thrombin (100 U/ml) from bovine plasma (Sigma-Aldrich) were separately dissolved in sterile PBS. Then, thrombin was mixed with 1ml of EGM-2 MV (Lonza) and placed on ice. Cells were detached and spun down at 1200 rpm for 5 min and cell pellet was resuspended in EGM-2 MV 4 U/ml thrombin. Cell suspension was mixed with fibrinogen (final concentration 3

mg/ml) at 1:1 volume ratio. The mixture was quickly pipetted into the gel filling ports. Devices were placed in a humidified enclosure and allowed to polymerize at room temperature (RT) for 15 min before the fresh medium was introduced to fluidic channels. iPSC-ECs medium was supplemented with 50 ng/ml of vascular endothelial growth factor (VEGF, Peprotech), for the first four days of culture. Medium for the tri-culture condition was supplemented with 1% (vol/vol) Astrocyte Growth factor (AGF, astrocyte growth supplement, ScienCell).

Three different cell combinations were tested: 1) iPSC-ECs mono-culture (6×10^6 cells/ml), 2) co-culture iPSC-ECs+PCs (add 2×10^6 cells/ml PCs) and 3) tri-culture of iPSC-ECs+PCs+ACs (add 2×10^6 cells/ml ACs). After fibrin polymerization, medium channels were coated for 30 min in an incubator (37°C 5% CO2) with human fibronectin (60 µg/ml) to promote endothelial cell adhesion. In each case, iPSC-ECs were subsequently seeded at $2x10^6$ cells/ml in EBM-2 (Lonza) into the fluidic channels to reduce diffusion of fluorescent dyes into the gel. Non-adherent cells were removed after 2 h. The device was kept in an incubator for 7 days (37 °C, 5% CO2), 200 µl of medium was replaced every 24 h. Devices prepared in this manner were used for both permeability measurements and immunocytochemical staining. PC conditioned medium was collected after 3 days, from a T75 flask of PCs culture, mixed 1:1 volume ratio with fresh medium and replaced every 24 h in the iPSC-ECs mono-culture in the microfluidic device.

The *in vitro* BBB model was developed by co-culturing human iPSC-ECs, and human brain PCs and ACs to mimic certain aspects of the organization and structure of the brain microcirculation observed *in vivo* (Fig. 1a,b). The BBB model formed by a vasculogenesis-like process, consisted of a well-connected and perfusable µVN in a microfluidic device (Fig. 1c, Supplementary Fig. 1a), interacting via paracrine, juxtacrine and mechanical signaling[38][39]. iPSC-ECs seeded in the side media channels reduced leakage through the side walls of the central gel region and promoted the formation of patent vessel connections to the media channels, facilitating flow into the network (Fig. 1d,e).

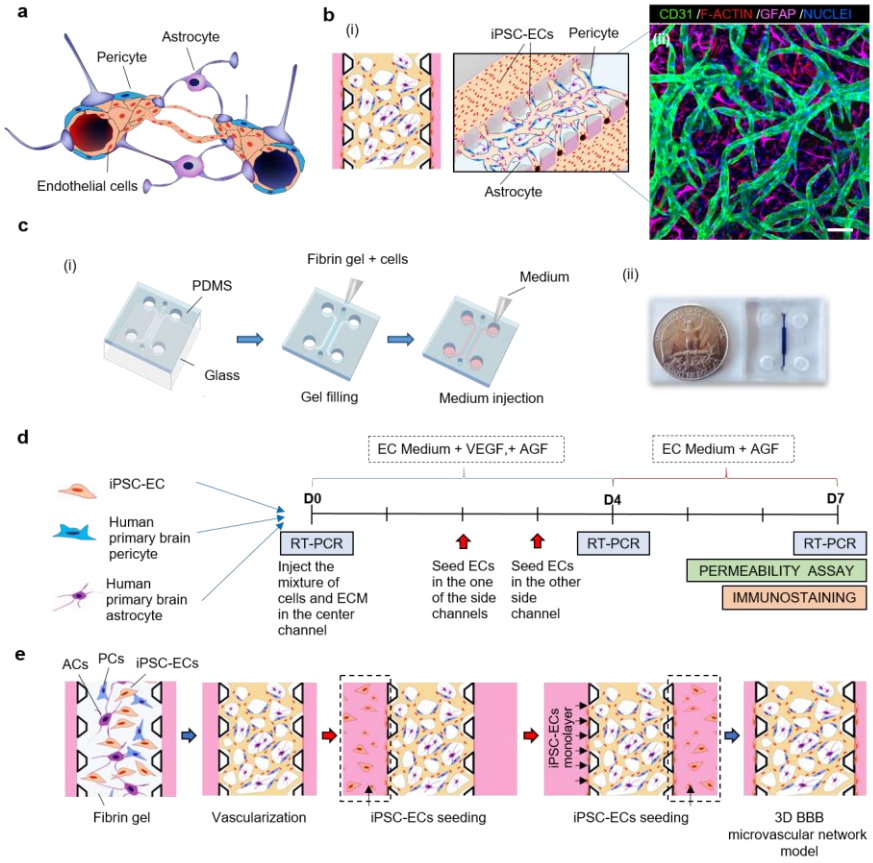

Figure 1: Blood-brain barrier and *in vitro* microvascular network model. (**a**) Schematic representation of the blood-brain barrier (BBB), composed of brain Endothelial cells (ECs) vessels overlapped by pericytes (PCs) and astrocytes (ACs) endfeet. (**b**, (i)) Schematic representation of proposed 3D BBB microvascular network (µVN) model that mimics the microvascular structure present in the brain environment. (**b**, (ii)) Confocal image of self-assembled BBB µVN model including iPSC-ECs (CD31, green), PCs (F-actin, red) and ACs (GFAP, magenta), and nuclei (DAPI, blue). (**c**) Microfluidic device fabrication: (**c**, (i)) PDMS mold with patterned channels were produced by soft lithography and bonded to a glass coverslip. The central gel region contained cells and hydrogels, side channels and reservoirs were filled with cell culture medium. (**c**, (ii)) A photo of the microfluidic device. (**d**) Timeline of the experiments. (**e**) Cell seeding configuration and experimental steps of vasculogenesis process of BBB µVN model including iPSC-ECs+PCs+ACs as self-assembled microvascular network and 3-dimensional ECs layer covering top, bottom and side surfaces of the fluidic channel. Scale bar (**b**, (ii)) indicates 100 µm.

Immunocytochemistry and confocal imaging

The 3D BBB µVNs were cultured for 7 days followed by rinsing in PBS and fixation in 4% paraformaldehyde (PFA, Electron Microscopy Sciences) for 15 min at RT. Cell membranes were permeabilized with 0.1% Triton X-100 (Sigma-Aldrich) for 5 min at RT and washed twice with PBS. Primary antibodies (1:100, volume ratio) against CD31, Glial Fibrillary Acidic Protein (GFAP), (Abcam), F-actin (Rhodamine Phalloidin, Molecular Probes), 4',6-Diamidino-2-Phenylindole (DAPI Thermo Fisher Scientific), were used to identify, respectively, iPSC-ECs, ACs, PCs, and nuclei. F-actin is strongly expressed in all cells present in our model, whereas only iPSC-ECs highly express CD31 and only astrocytes express GFAP. We therefore used double staining of CD31/F-actin to identify iPSC-ECs and GFAP/F-actin to identify ACs, which enabled us to clearly identify the PC population as those cells that only express F-actin.

To characterize the presence of TJs and ECM proteins by immunocytochemistry, primary antibodies were used against: ZO-1 (Invitrogen), occludin, claudin-5, laminin and collagen IV (Abcam). Secondary antibodies (1:200, volume ratio) were anti-rabbit or anti-mouse IgG conjugated with Alexa Fluor (488-555, or 647) (Invitrogen). Detail on primary and secondary antibodies are listed in Supplementary Table 2. Devices were incubated with primary and secondary antibodies overnight at 4°C, placed on a shaker. After PBS washing, devices were imaged using a confocal laser scanning microscope (FMV-1000, Olympus, Japan) (aspect ratio 1024×1024) high resolution images at 10us/pixel scan velocity. Phase contrast imaging was used for morphological observations at different culture time-points (Axiovert 200, Zeiss, Germany). Post-processing and stitching for tiled images were performed using Imaris (Bitplane, Switzerland) and Fluoview (Olympus, Japan). Fold change average immunofluorescent (IF) intensity (relative to iPSC-ECs) was calculated by dividing total immunofluorescent intensity by cell boundary length (ZO-1, occludin, and claudin-5) or by vascularized area (laminin, collagen IV). ROIs were selected to contain only microvascular portions such that no part outside the vessels were included in the computations.

205

206 **Characterization of BBB microvascular parameters**

207 To characterize microvascular parameters, confocal images were analyzed using ImageJ software
208 (http://rsbweb.nih.gov/ij/) and plugins (Trainable Weka Segmentation 3D, 3D geometrical measure).
209 Briefly, raw images were prepared by enhancing contrast and removing noise. An automatic threshold
210 was used to produce binarized images. From 2D projections, lateral vessel area ($A_{lateral}$), and total
211 branch length (L_{branch}) were computed by ImageJ. Percentage of area coverage was calculated
212 dividing $A_{lateral}$ by the entire area of the region of interest. Taking advantage of the observation that
213 most vessels are oriented in a plane parallel to the glass substrate, lateral diameters, parallel to the
214 glass substrates of the devices, were computed as the ratio of the projected lateral vessel area to the
215 total branch length. Transverse diameters, perpendicular to the glass substrate, were computed using
216 the 3D vessel volume (V) and the surface area of the vessels in 3D ($A_{surface}$). Average cross-section
217 area and circularity were computed using lateral and transverse diameters. The sequences of
218 instructions and equations used to compute both diameters, cross-section, lateral and surface areas
219 and circularity are shown in Supplementary methods.

220

221 **Microvascular network perfusion and fluorescent dextran-based permeability assay**

222 To assess permeability of the 3D BBB model, solutions containing 10 or 40 kDa FITC-dextran
223 (Sigma-Aldrich) were introduced as fluorescent tracers, and time-sequential images to assess leakage
224 through the microvascular barrier were captured. Briefly, after 7 days of culture, each device was
225 moved to the confocal conditioning chamber (37°C, 5% CO_2), culture medium was aspirated from
226 all reservoirs in each side channel. Then, 5 µl of dextran solution in PBS was injected in one side,
227 simultaneously with 5 µl of medium on the other fluidic channel to maintain equal hydrostatic
228 pressures in the device. Confocal images were acquired every 3-5 min for 6 to 8 times to create the

entire 3D stack of the gel volume with microvascular formation at each time point. ROIs were selected considering vascular networks with a clear boundary between vessel wall and gel regions.

To assess perfusability, fluorescent tracers (FITC-dextran) were introduced through the microvascular networks by imposing a hydrostatic pressure drop across the gel region between two medium channels. Videos were recorded using NIS-Elements software (NIKON) on a fluorescent microscope (Nikon, TI-E ECLIPSE.) at 30 frames per second.

Quantification of vessel permeability coefficient

The vascular permeability is evaluated as the flux of solute across the walls of the vascular network. Using mass conservation, the quantity of FITC-dextran crossing the vascular network equals the rate at which it accumulates outside the vessels in the tissue gel region. According to a previously described method[40], vascular network permeability, P_v, was quantified by obtaining the average intensity of vessels I_v and tissue (outside vessels) I_T at two different time points *t1* and *t2* and using:

$$P_v = \frac{1}{(I_V^{t1} - I_T^{t1})} \frac{(I_T^{t2} - I_T^{t1})}{\Delta t} \frac{V}{A_{surface}}$$

Here, Δt is the time between two images, V is the tissue volume, $A_{surface}$ is the surface area of all vessels in the selected ROI, computed based on the assumption that the ratio $V/A_{surface}$ can be estimated as the tissue area $A_{lateral}$ divided by the perimeter of the vascular region L_{branch} in the projected 2D images from the 3D confocal stacks. Diffusion of fluorescent dextran into the gel was minimized by introducing an iPSC-ECs monolayer in both side channels. The fluorescence intensity values, vessel surface area and tissue/gel region area were computed using ImageJ.

252 **RNA isolation and quantitative RT-PCR**

253 Total RNA was isolated from different conditions using TRIzol reagent (Life Science) for dissolving
254 fibrin gel. Reverse transcription was performed using SuperScript VILO cDNA synthesis kit
255 (Invitrogen). Quantitative Real-time RT-PCR (RT-PCR) using SYBR Premix Ex Taq (Takara) or
256 Power SYBR Green PCR Master Mix, was performed with a 7900HT Fast Real-Time PCR System
257 (Applied Biosystems). mRNA of endothelial cell adhesion molecule (PECAM-1) also known CD31,
258 glyceraldehyde 3-phosphate dehydrogenase (GAPDH) and Ribosomal Protein S18 (RPS18) were
259 used as housekeeping genes, set to 100% as the internal standard. RT-PCR experiments were repeated
260 at least 3 times for cDNA prepared from 6 devices. Primer sequences (Integrated DNA technology)
261 are listed in supplementary Table 1. RT-PCR was performed in a scaled up version a of the device
262 (Supplementary Fig. 1b) in order to collect higher amount of total RNA.

263

264 **Statistical analysis**

265 All data are plotted as mean ± SD. One-way ANOVA with pairwise comparisons by the Tukey post
266 hoc test was used to determine whether three or more data-sets were statistically significant. Statistical
267 tests were performed using JMP pro (SAS Institutes, Inc.). At least four devices (≥2 regions per
268 device) for each condition within 3 independent experiments were used for the imaging and data
269 analysis. **** denotes $p < 0.0001$, *** denotes $p < 0.001$, ** denotes $p < 0.01$, * denotes $p < 0.05$.
270 Non-paired student's t-test was used for significance testing between two conditions.

271

Results

Optimization of self-assembled microvasculature

Three models were established, as described in Methods, with progressively greater complexity: (i) iPSC-ECs (Fig. 2a,b (i)), (ii) iPSC-ECs + PCs (Fig. 2a,b (ii)), and (iii) iPSC-ECs + PCs + ACs (Fig. 2a,b (iii), Supplementary Figs. 4a-c). In each case, the iPSC-ECs elongated and intracellular intussusception and vacuoles appeared after 1 day followed by the formation of lumen structures after 2-3 days (Supplementary Figs. 2a and 3a,b). Further development of the μVNs resulted in a highly interconnected microvasculature by day 7 of the culture (Fig. 2b).

With iPSC-ECs alone (Fig. 2a,b (i)), vascular networks formed in 4-5 days (Supplementary Fig. 2a), however, the vessels fused, forming large, elliptical cross-section lumens, many of which contacted the bottom coverslip (Fig. 3a) and gradually degraded and regressed after 7 days (Supplementary Fig. 5a). In contrast, co-culture of iPSC-ECs with PCs formed smaller and more highly branched vessels (Figs. 2a,b (ii), 3b). No significant difference could be observed when iPSC-ECs were cultured alone or with PC conditioned medium (Supplementary Fig. 5b), suggesting that contact with PCs effectively facilitated endothelial organization, by stabilizing a mature vasculature with a morphology more similar to that found *in vivo.*

The addition of ACs further assisted in the development of a complex inter-connected and branched architecture found in native vasculatures (Fig. 2a,b (iii), Supplementary Fig. 3a,b). In tri-culture with ACs, the μVNs exhibited distinctive behavior during formation, with increased tortuosity and vessels extending higher up in the 3D gel (Fig. 3c). A fundamental characteristic of the BBB is the stratified organization of cells around the vessels and their direct contact interactions. In 4 replicates with 10-12 high resolution confocal images, we observed a spontaneous self-organization into multicellular BBB structures. Indeed, PCs (F-actin, red, Fig. 2c) adhered to both sides of the endothelial cell

Commentato [CM1]: If reviewer would like to specify how many biological replicates/highly resolution confocal, numbers are more than 4 replicates with 10-12 images.

surface, surrounding the vessel (CD31, green, Fig. 2c,e, Supplementary Fig. 6a, Supplementary video 1). For example, tracing the intensity profiles of EC and PC fluorescence (Fig. 2d), F-actin expression was observed outside the vessel, clearly delineating the presence of PCs. These results showed that pericytes partially overlapped the outer surface of the EC layer exhibiting a BBB-like organization. In addition, 3D rendering of vessel bifurcations showed PCs in contact with the endothelium at multiple locations (Fig. 2e). Moreover, direct physical contacts were observed between AC endfeet (Glial Fibrillary Acidic Protein, (GFAP), violet) and the abluminal surface of the brain vessels (CD31, green, Fig. 2f; Supplementary Figs. 6b,c).

Characterization of microvascular parameters

To determine the geometrical changes in the μVNs (Fig. 3a-c, Supplementary Fig.4a-c), lateral and transverse vessel diameter distributions, percentage of image area containing vascular networks, and total branch length were each quantified (Fig. 3d-i). As expected, in the iPSC-ECs+PCs co-culture, the lateral vessel diameters (30 to 100 μm, Fig. 3e (i)) were significantly lower than in mono-culture conditions (50 to 150 μm with a few outliers to 200 μm, Fig. 3d (i)). Lateral diameters were further reduced by adding ACs (most values between 25 and 50 μm (Fig. 3f (i))). The overall transverse diameter distributions were similar for all three conditions, ranging between 10 and 40 μm, and centered around 30 μm (Fig. 3d-f (ii)).

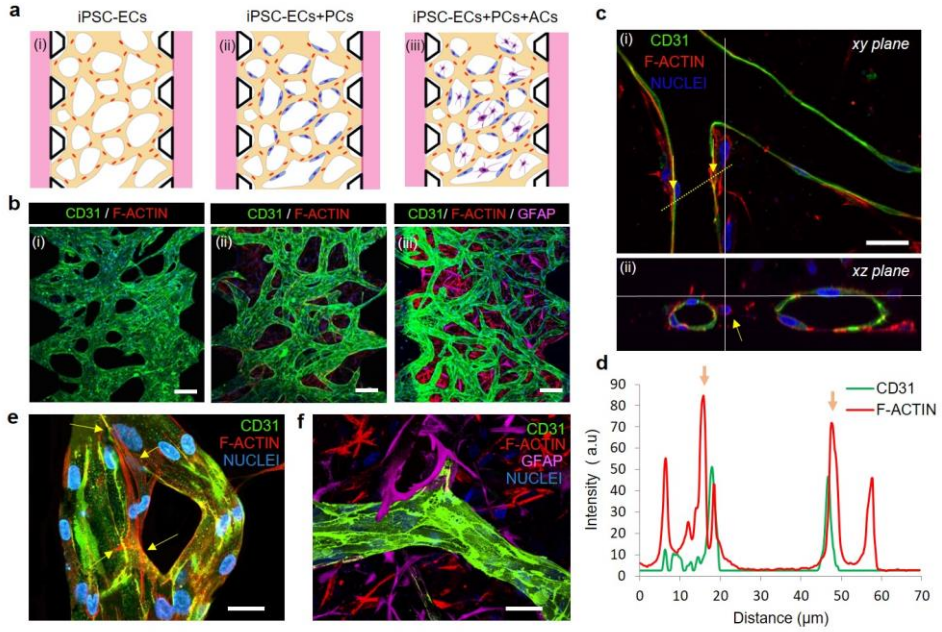

316

317 **Figure 2: Microvascular network conditions iPSC-ECs - PCs/ACs contact interactions.** (**a**)
318 Schematic representation and (**b**) confocal images of (**a, b**, (i)) iPSC-ECs mono-culture (CD31,
319 green), (**a, b**, (ii)) co-culture with PCs (F-actin, red), and (**a, b**, (iii)) tri-culture with PCs and ACs
320 (GFAP, magenta), after 7 days of culture in the microfluidic device. (**c**) Cross-sectional images of
321 blood microvessels showing hollow lumens. (**c**, (i)) PCs adhered to and partially enveloped brain
322 microvessel. (**c**, (ii)) Cross-sectional images of blood microvessels showing a lumen enclosed by
323 iPSC-ECs and PCs. PCs surround the blood vessel. Image shows how section was sampled using a
324 line scan measurement (yellow line) and generation of intensity profile histogram. (**d**) Intensity
325 profile analysis of CD31/F-actin in iPSC-ECs -PCs interaction corresponding to the yellow line scan.
326 Intensity profile shows distinct peaks (yellow arrow) at the position of contact interaction/overlapping
327 between ECs and PCs. CD31 expression (green) was low when F-actin expression (red) was high,
328 further indicating that F-actin expression belonged only to brain PCs outside the vessels. Region of
329 low green intensity corresponds to the vascular bed of the vessel. (**e**) Contact interactions of PCs
330 enveloping blood microvessel. PCs adhered to and partially enveloped brain microvessel. (**f**)
331 Confocal image of iPSC-ECs, PCs and ACs in the tri-culture condition. Images were analyzed using
332 Imaris 8.3. Scale bars indicate 100 µm (**b**) and 20 µm (**c**, **e**, **f**).

333

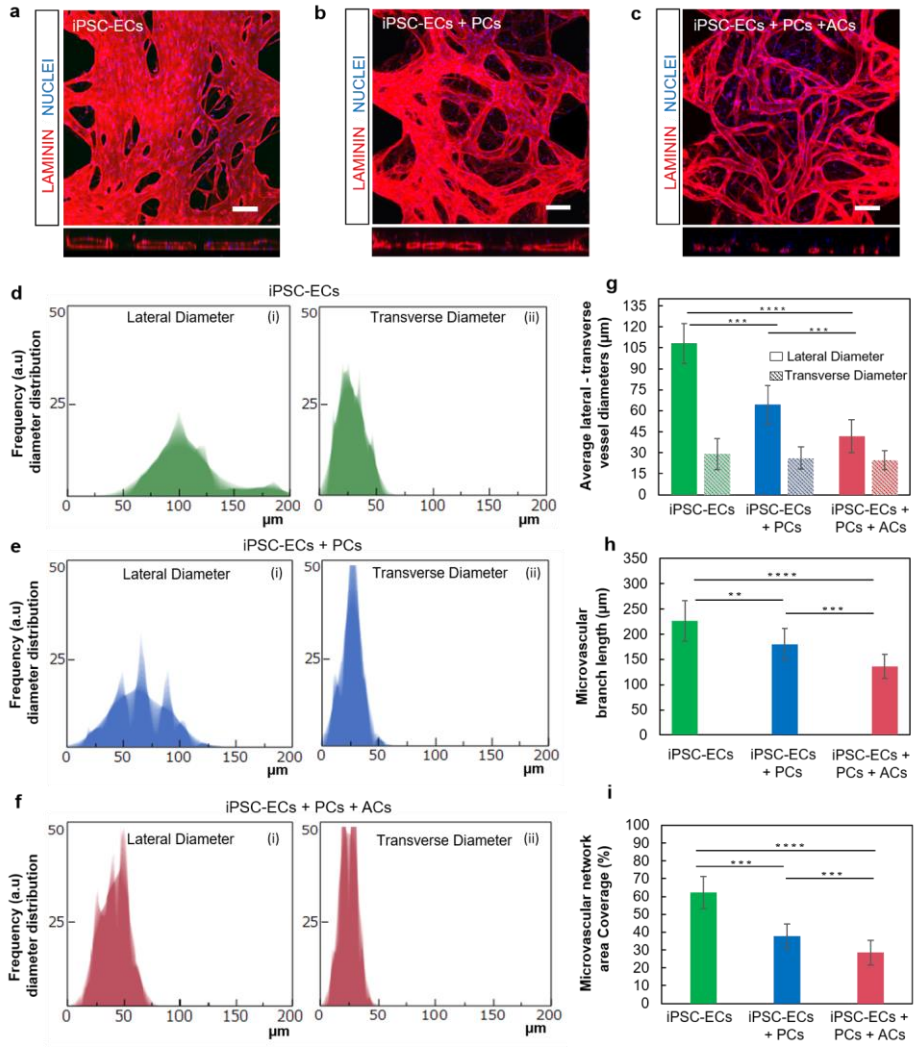

Figure 3: 3D BBB microvascular network parameter quantification. Confocal images of laminin expression (red) and nuclei (DAPI, blue) of 3D BBB µVN maturation from (**a**) mono-culture of iPSC-ECs, (**b**) co-culture of iPSC-ECs+PCs and (**c**) tri-culture of iPSC-ECs+PCs+ACs (scale bar: 100 µm). Distribution of lateral and transverse vessel diameter measurements of 3D BBB µVNs formed by vasculogenesis, for (**d**) mono-culture of iPSC-ECs, (**e**) co-culture with brain PCs, (**f**) tri-culture with brain PCs and ACs. Additional image in supplementary Fig. 4. (**g**, **h**, **i**) Quantification of microvascular network parameters: (**g**) average lateral and transverse vessel diameters in each condition, (**h**) microvascular branches average length and (**i**) percentage ratio of microvascular network area coverage to the total area. * p<0.05, ** p<0.01, *** p<0.001, **** p<0.0001. Error bars ± SD, n=30.

Hence, lumens with nearly circular cross-section and consequently smaller cross-section area and higher circularity (Supplementary Fig. 6d-f) formed in the tri-culture condition (average lateral diameter: 42 ± 13 μm, average transverse diameter: 25 ± 6 μm, Fig. 3g), while lumens were flattened and had elliptical cross-section in mono-cultures (average lateral diameter: 108 ± 14 μm, average transverse diameter: 29 ± 10 μm, Fig. 3g), and in co-cultures (average lateral diameter: 64 ± 13 μm, average transverse diameter: 27 ± 7 μm, Fig. 3g).

Moreover, the cumulative average μVN branch length decreased from mono-culture (226 ± 40 μm), to co-culture (179 ± 31 μm), and tri-culture (136 ± 24 μm) conditions, respectively (Fig. 3h), demonstrating a highly complex and intertwined vascular network. Accordingly, the networks with iPSC-ECs, iPSC-ECs+PCs, and iPSC-ECs+PCs+ACs conditions covered progressively less area in the projected image (62%, 42%, and 28%, respectively (Fig. 3i). Indeed, in tri-culture conditions, the μVNs showed improved morphology provided by the co-culture with ACs and PCs, with reduced vessel diameters and average branch length. These results mirror similar observations that have been attributed to the secretion of angiogenic growth factors by PCs and ACs [19][20].

In summary, these results indicate that the networks formed with all three cell types --iPSC-ECs+PCs+ACs -- contained more stable and shorter vessel branches, with more circular cross-sections and smaller vessel diameters compared to the other conditions. These networks also exhibited more random interconnections and improved 3D structural orientation into the gel region: such structure is more similar to *in vivo* vessel morphology [30].

Protein synthesis and gene expression related to blood-brain barrier (BBB)

To analyze whether the engineered 3D brain microvascular model constitutes a functional barrier and exhibits physiological characteristics typical of the BBB present *in vivo*, we validated and compared

protein expression measured by immunocytochemistry assays and quantitative real-time RT-PCR, performed after 7 days. Firstly, immunocytochemistry images of vascular networks obtained under different culture conditions were compared from multiple regions of interest (ROIs) within the vessels. The expression of endothelial-specific junction proteins ZO-1, occludin, and claudin-5 (Fig. 4a-c), and ECM constituents such as laminin (Fig. 4d) and collagen IV (Fig. 4e) was analyzed by confocal microscopy (See also Supplementary fig. 7b-f). Interestingly, the increase of TJ protein expression in µVNs was observed by introducing PCs and ACs (Fig. 4a-c). Therefore, the BBB µVNs obtained by iPSC-ECs+PCs+ACs tri-culture (Fig. 4a (iii)) relatively expressed much higher level of ZO-1, occludin and claudin-5 compared to mono-culture of iPSC-ECs and iPSC-ECs+PCs (Fig. 4a-c). Quantitative analysis of fold change average immunofluorescent (IF) intensity (relative to iPSC-ECs) confirmed qualitative observations (Fig. 4f). Average immunofluorescent (IF) intensity was calculated by dividing the total immunofluorescent intensity by the cell boundary length in each ROI in the case of tight-junction proteins (ZO-1, occludin, and claudin-5). In the case of basement membrane protein deposition (laminin, collagen IV), average IF intensity was calculated by dividing the total IF intensity by the vascularized area in each ROI. ROIs were selected to contain only microvascular portions (Fig. 4f). Continuous cell-cell junctions lining the rhomboidal boundaries of endothelial cells along lumens were observed in co-culture and tri-culture conditions, as demonstrated by the clear delineation of ZO-1 along the cell-cell border (Supplementary Fig. 7a).

Another sign of vessel maturation was the deposition of basement membrane proteins, exhibiting a similar trend to TJ expression. Laminin and collagen IV immunofluorescence intensity (Fig. 4d-f) approximately doubled in the case of the microvascular networks obtained by iPSC-ECs+PCs+ACs tri-culture (Fig. 4d,e (iii)) compared to iPSC-ECs mono-culture (Fig. 4d,e (i)) and was significantly higher than for iPSC-ECs+PCs co-culture (Fig. 4d,e (ii)).

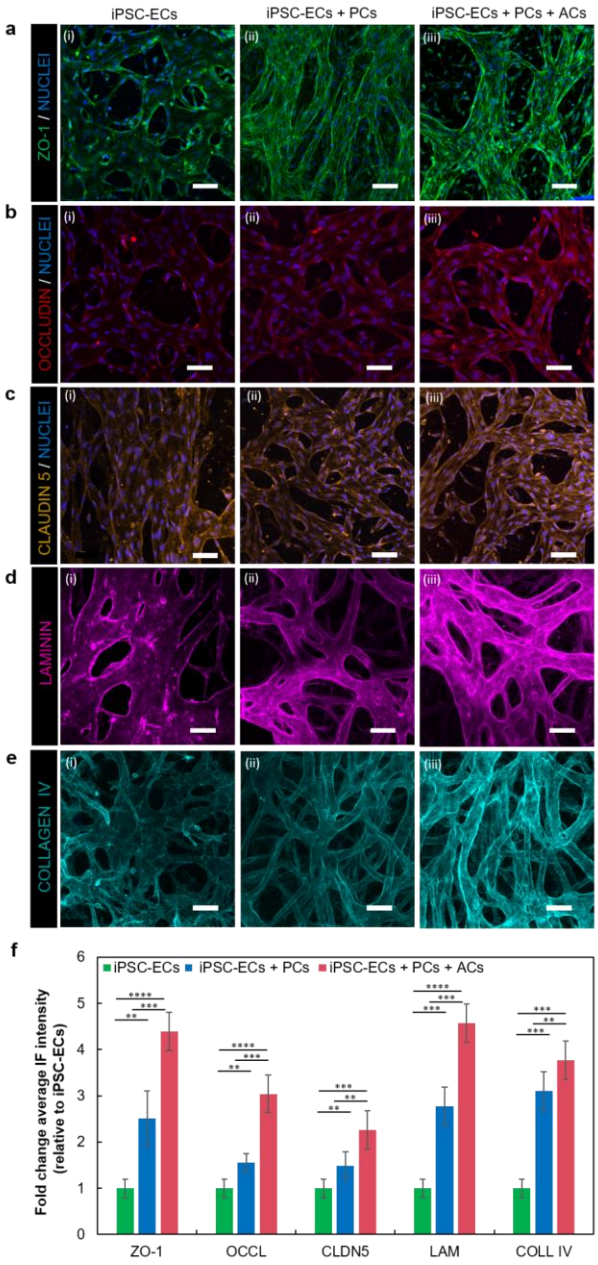

Figure 4: Immunocytochemistry analysis of tight junctions and ECM deposition. Self-assembled microvascular networks formed after 7 days in microfluidic device culture for: (i) mono-culture of iPSC-ECs, (ii) co-culture with PCs and (iii) tri-culture with PCs and ACs (BBB microvascular network model). (**a**-**e**) Microvascular networks were immunostained for tight junctions (ZO-1, occludin (OCCL) and claudin-5 (CLDN 5)), and ECM production (laminin (LAM) and collagen IV (COLL IV)), and nuclei (DAPI) inside microfluidic devices and imaged by confocal microscopy. (**a**) Immunofluorescent (IF) intensities of ZO-1 were well-defined in co-culture and tri-culture conditions. ZO-1 expression was clearly localized at the intersection between cells forming a rhomboidal grid, characteristic of mature and well-organized microvasculature. Instead, monoculture exhibited low expression of TJ proteins with no visible and defined accumulation at cell boundaries. Similar behavior was exhibited by (**b**) occludin and (**c**) claudin-5. (**d**) Confocal images of deposition of laminin and (**e**) collagen IV showed production and remodelling of a distinct ECM by the different microvascular networks. BBB microvascular model with PCs and ACs expressed higher intensities of laminin and collagen IV compared to monoculture and co-culture, providing evidence that PCs and ACs improved vascular function. Qualitative image tests were realized by ROI intensity analysis. (**f**) Fold change average IF intensity (relative to iPSC-ECs) quantify the protein expression according to the IF images. Computed image intensities were normalized by the selected area. * $p<0.05$, ** $p<0.01$, *** $p<0.001$, **** $p<0.0001$. Error bars ± SD, $n=8$. Confocal image scale bar: 50 µm.

To confirm immunocytochemistry results, total RNA was extracted from the total cell population in the microfluidic device (Fig. 5a) and purified from different conditions at several time points (day 0, 4, and 7). RT-PCR analysis was conducted considering gene markers of TJ proteins, ECM production and several endothelial membrane transporters such as efflux-pumps, passive transports, solute carriers, and receptor-mediated mechanisms. Vessel maturation was investigated in terms of the expression of several markers and proteins, in the case of co-culture and tri-culture conditions, and was compared to the control condition (iPSC-ECs). The mRNA expression of each gene was measured relative to the expression of CD31 and GAPDH (fold change). TJ proteins such as ZO-1, occludin, and claudin-5 were highly up-regulated in the tri-culture condition at day 7 compared to mono-culture and co-culture conditions. Interestingly, the expression of TJ markers in the tri-culture case increased as a function of culture time (Fig. 5b, Supplementary Fig. 10a-e). As expected, GFAP was regulated exclusively in the presence of ACs. PDGFR gene expression was slightly higher in the tri-culture condition while alpha-smooth muscle actin (αSMA) expression was reduced, possibly due to the increased proliferation of iPSC-ECs and PCs stimulated by ACs. Furthermore, basement membrane proteins (collagen IV, laminin) were highly expressed over time in the tri-culture condition compared to the mono- and co-culture cases. In addition, gene expression of several BBB-specific membrane transporters and receptors which exploit several transport mechanisms (passive diffusion, ATP-binding efflux transporter, solute carriers and receptor-mediated transcytosis), such as P-GP, MRP1, MRP4, TF-R, LRP1, LAT-1, GLUT-1, CAT1, MCT1, ABCA1, and BCRP widely increased over time in the tri-culture BBB model (iPSC-ECs+PCs+ACs), compared to iPSC-ECs+PCs and iPSC-ECs microvascular network conditions. Overall after 7 days, the tri-culture condition displayed a constantly increased maturation and upregulation of all examined genes (Fig. 5b, Supplementary Fig. 10a-e, Primer sequences in Supplementary Table 1).

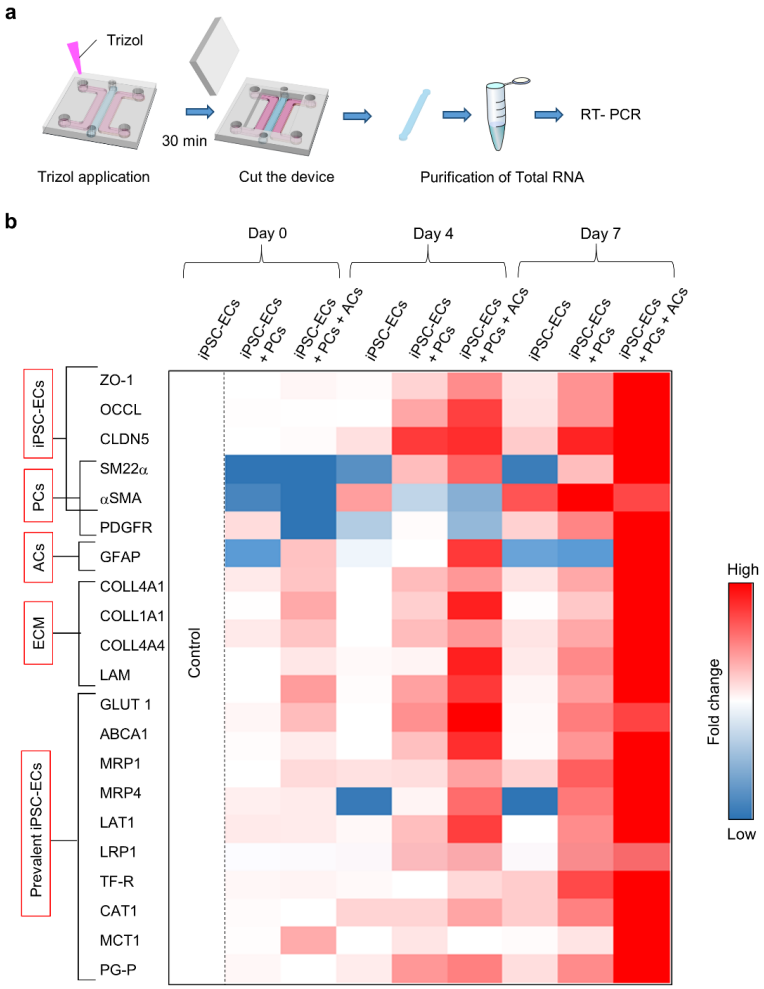

Figure 5: Quantitative relative RT-PCR of 3D BBB µVNs in microfluidic device. (**a**) Schematic representation of vascular network and gel extraction from a microfluidic device, purification of total RNA and conduct of RT-PCR experiments. (**b**) Heatmap of RT-PCR results of mono-culture of iPSC-ECs, co-culture with PCs, and tri-culture with PCs and ACs at 0, 4 and 7 days. Relative comparison of mRNA expression of factors relating to microvascular maturation and other typical BBB features. Gene analysis considered markers 1) expressed in ECs, 2) expressed in PCs, 3) expressed in ACs, 4) ECM protein RNA, and 5) genes expressed predominantly by ECs, but also in smaller amounts by the other two cell types. Fold change was relative to control (mono-culture of iPSC-ECs, day 0). The internal standard housekeeping gene was CD31. $0.01 < p < 0.05$, $n = 3$.

Distinct cell contributions to BBB permeability

The permeability of the microvessels in our BBB μVN models was computed to assess the practical potential to use our system to mimic solute transport *in vivo.* In all culture conditions, vessels comprising the entire vascular network were well formed and completely perfusable at day 7 (Supplementary Fig. 8d, Supplementary video 2, 3). Permeability coefficients were measured by introducing solutions containing FITC-dextran tracers in the vasculature (10 & 40 kDa), and capturing confocal images at 5 min intervals and computing themed as explained in Methods (Fig. 6a-d, Supplementary Fig. a-c). With side-channels seeded with iPSC-ECs, permeability to 40 kDa FITC-dextran of the μVN obtained under mono-, co-, and tri-culture conditions progressively decreased: 6.6, 2.5, and 0.89 $\times 10^{-7}$ cm/s, respectively. A similar trend was observed for the 10 kDa FITC-dextran: 12, 4.8 and 2.2 $\times 10^{-7}$ cm/s, respectively (Fig. 6e, f). When iPSC-ECs were not added to the side channels, leakage of tracer across the side-walls of the gel region gave rise to higher permeability values, roughly a two-fold increase, due to the artifact associated with the additional source of tracer influx. Side channel seeding helped in several ways. It improved coverage of the exposed side gel surface with an endothelial monolayer, filled gaps that sometimes formed at the gel-post borders, and increased the number and patency of connections between the networks and the main channel (Fig. 7a and Supplementary Fig. 9a-e).

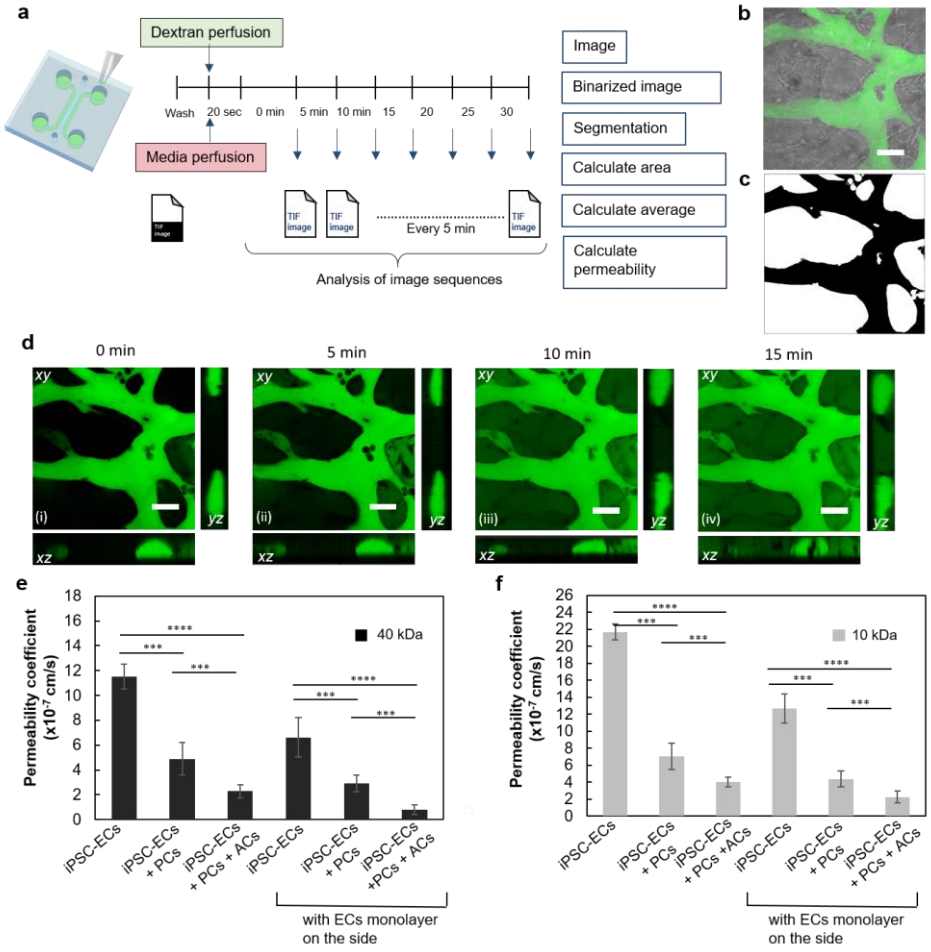

Figure 6: Permeability assay in BBB model. (**a**) Timeline of permeability experiments and computational analysis. After cell culture medium was removed, dextran solution was injected and image stacks were captured every 3-5 mins for 30 mins. Workflow of image analysis by ImageJ and permeability coefficient calculation. (**b**) Confocal and bright field images at time 0. (**c**) Image binarization after thresholding to identify vessel borders. (**d**, (i-iv)) Maximum image projections and cross-sections including xy, xz and yz planes at 4 time-points. The graphs show permeability coefficients for 3 different conditions (with and without ECs seeding in side channels) using (**e**) 40 kDa and (**f**) 10 kDa FTIC-dextrans in mono-culture of iPSC-ECs, co-culture of iPSC-ECs+PCs, and tri-culture of iPSC-ECs+PCs+ACs. The data show mean value, error bars ± SD, n=10, * p<0.05, ** p<0.01, *** p<0.001, **** p<0.0001, scale bars 50 µm.

a

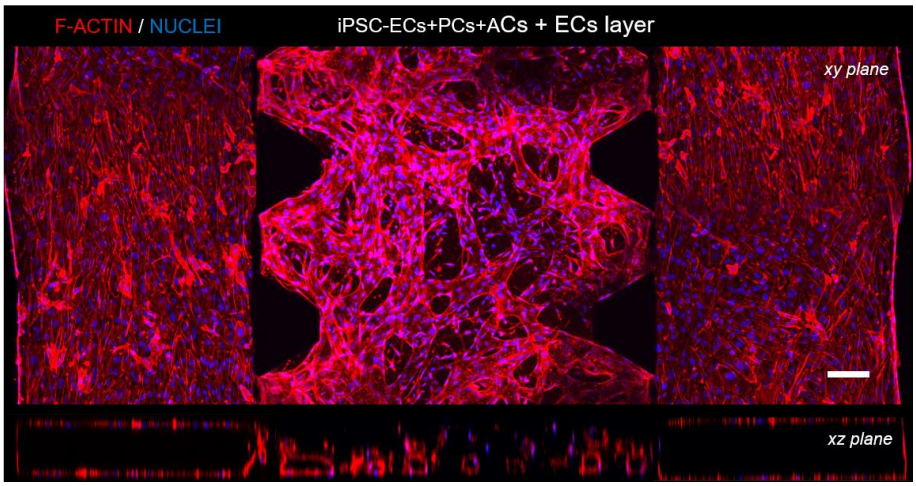

Figure 7: BBB microvascular network model. (**a**) Confocal images of xy and xz (cross-section) planes of the 3D BBB microvascular *in vitro* model with iPSC-ECs+PCs+ACs, including EC layers in the side channel. Scale bars 200 µm.

Discussion

In this work, we developed a new *in vitro* human BBB microvascular model consisting of a self-assembled µVN of iPSC-ECs co-cultured with brain PCs and ACs. Novelty of our microfluidic platform arises from simultaneous seeding of three human cell types into a single gel region, producing a perfusable vascular network, with permeabilities lower than those of other published microfluidic models [23][24][27][32][34].

iPSC-ECs were selected as they are immature endothelial cells, capable of organizing into a complex and perfusable vascular network [41], with lower permeability values compared to other non-brain EC models [42][43][44]. The potential features of iPSC-ECs may contribute to a coherent and relevant replacement of "brain" endothelial cells to establish a 3D BBB microvascular model. Moreover, iPS cells may be potentially derived from patients who suffer from specific neurodegenerative diseases [45], thereby producing a pathological model to study disease progression, to screen for drugs appropriate for patients' sub-groups, or even for precision medicine applications to select optimal, personalized therapies.

Our 3D BBB µVN model incorporating three cell-types (Fig. 1b and Fig. 7a) expressed both functional and morphological characteristics present in the human BBB, with stable and perfusable µVNs, comprising small lumens with circular cross-section comparable with *in vivo* human microcirculation (arterioles and venules <100 µm; capillaries <10 µm) [28][29]. It also defined microvascular branch length similar to segments in close proximity to the third ventricle (caudate, putamen, and thalamus with an average of 70 µm) [46] and characterized by low permeability and transport selectivity (Fig. 6e,f and Supplementary movie 2, 3). It draws upon the intrinsic nature of ECs interacting with other neural cell types to recapitulate brain vascular morphogenesis during developmental process via vasculogenesis [47][48], in which immature ECs recruit PCs and ACs to

form new vessels through PDGFR and Sonic hedgehog (SHH) signaling pathways [47][49]. In particular, PCs played an important role to create a robust and stable vessel network with significant lateral diameter reduction (Fig. 3d,g). It has been previously demonstrated that ECs need a combination of juxtacrine and paracrine signaling to create a stable and physiologically-relevant microvasculature on a chip [38][39]. Hence, the resulting formation of a physiologically-relevant microvasculature, was facilitated by juxtacrine interactions and paracrine signaling between iPSC-ECs and PCs (enveloping the endothelium) (Fig. 2c-e), along with the increase of TJ expression and appropriate concentration of growth factors (Fig. 4a-c, Supplementary Figs. 7a-d, 10a-d). Indeed, improvements were associated with the presence and secretion of vascular endothelial growth factor VEGF (50 ng/ml in the supplemented medium), angiopoietin-1 (ANG-1) and fibroblast growth factor (FGF) by stromal cells, especially PCs [50]. However, as VEGF could modulate vascular permeability through the disruption of tight junctions and consequent break down of the BBB [51], cell culture medium was supplemented with VEGF up to day 4.

We hypothesize that this morphological change in the final structure of the BBB μVNs was induced by not only the presence and cell-secretion of pro-angiogenic and vasculogenic growth factors and ECM proteins, but also by juxtacrine signaling, consistent with previous findings [35][52][53]. Our results also suggest that PCs not only influence the creation of vascular networks but also induce the differentiation of iPSC-ECs into brain-specific endothelial cells, as determined by the RT-PCR results (Fig. 5b, Supplementary Fig. 10a-d). Indeed, it has already been shown that co-culture of ECs with PCs is required for BBB formation and the maintenance of homeostasis by contact and paracrine interactions [54].

In addition to the contribution of PCs, ACs also improved BBB formation and integrity. iPSC-ECs self-assembled into mature vascular networks forming complex structures when interacting with both cell types. The role of ACs was evidenced by an increase in the expression of BBB transporters and

560 TJ proteins, such as ZO-1, occludin, claudin-5, ECM deposition (Figs. 4a-e, 5b, Supplementary Fig.
561 7a-c), and the corresponding decrease in permeability, (Fig. 6e-f) similar to previous transwell and
562 microfluidic-based models incorporating ACs [55]. In particular, the upregulation of typical BBB
563 transporters such GLUT-1, LAT-1, PG-P, TF-R, LRP1 and MRPs is fundamental to obtain an *in vitro*
564 BBB model for drug design and testing. Indeed, these specific transporters were highlighted as
565 potential targets to enhance the penetration of drugs into the brain [56] (Supplementary Fig. 10d).
566
567 In our model, AC endfeet were directly attached to the surface of vascular networks in the 3D matrix
568 (Fig. 2f, Supplementary Fig. 6b,c). This morphological feature of ACs recapitulates their
569 physiological arrangement in the brain and provides mutual biochemical support for those cells,
570 helping to maintain the integrity of the neurovascular networks [57]. Our findings suggest that the
571 addition of ACs is in part responsible for the improved morphology of BBB anatomical structure.
572 They might also contribute through paracrine signals to the development of a BBB-like endothelial
573 phenotype since ACs are known to regulate influx/efflux, vasodilatation/vasoconstriction by inducing
574 tightening of the endothelium [19], as well as cytokine and growth factor secretion such as basic FGF,
575 glial-derived neurotrophic factor (GDNF), and ANG-1 [58]. Further investigation is needed to
576 ascertain the relative importance of different biological pathways and factors improving BBB
577 integrity, however, direct adhesion of ECs, PCs and ACs might facilitate N-cadherin cell-cell
578 interactions [47].
579
580 As key features in assessing the value of BBB microvascular models for drug transport studies,
581 vascular perfusability and permeability were measured using fluorescent probes. The vessel networks
582 in our tri-culture BBB model attained permeability values of 8.9×10^{-8} cm/s and 2.2×10^{-7} cm/s for 40
583 kDa and 10 kDa FTIC-dextran, respectively (Fig. 6e,f), confirming barrier selectivity depending on
584 their molecular weight [59].
585 Importantly, these values are comparable to those measured *in vivo* in rat cerebral microcirculation

586 ($3.1 \pm 1.3\times10^{-7}$ cm/s for a 10 kDa FITC-dextran) [60], ($1.37\pm 0.26\times10^{-7}$ cm/s for a 40 kDa FITC-
587 dextran) [61], and similar to specific models that employ brain ECs derived from iPSCs (IMR90-4)
588 by co-culturing with astrocytes and/or neurons [62][63], and lower than previously reported 3D
589 [23][27][32][34], or 2D BBB models [24][64].
590
591 As a side note, inclusion of an iPSC-EC monolayer in the adjacent fluidic channels improved vascular
592 perfusability and also reduced the artifacts associated with tracer leakage across the sidewalls of the
593 gel region (Fig. 7, Supplementary Fig. 9a-e). Consistent with the progressive reduction in
594 permeability with increasing model complexity, we observed a corresponding increase in the tightness
595 of junctional proteins and their regulation [53][65], evaluated by immunostaining and RT-PCR
596 analysis. This contrasts with a previous study that reported an increase in permeability coefficient
597 when human brain endothelial cells (hCMEC/d3) were co-cultured with ACs isolated from rats [32],
598 possibly due to cross-species effects, as suggested by the authors of [29].
599
600 It is important to note that our model lacked neurons and microglia, and these might have further
601 effects on barrier functionality. Recent literature has shown that the upregulation of BBB-specific
602 transporters and the differentiation of brain-specific ECs are induced by the co-culture of iPSC-ECs
603 with iPS derived neurons [66]. In the same model authors demonstrated the possibility of drug
604 screening using iPSC-ECs in combination with all human iPS derived cells using transwell methods.
605 Also, co-culture with neural iPSCs has been found to improve EC barrier integrity and decrease
606 vascular permeability [66]. Therefore, there appear to be additional advantages gained by an even
607 more comprehensive human patient-derived *in vitro* model [66], combining iPSCs and/or neural stem
608 cells with the vascular networks, PCs, and ACs described here. Moreover, using iPS cells derived
609 from patients affected by neurological disorders [45], such as Alzheimer's disease, a BBB
610 pathological model could be obtained.
611

Our 3D self-organized system has several advantages compared to the *in vitro* 2D membrane-based monolayer, including its more physiologically-relevant morphology. Permeability measurements, however, at this point are limited to quantifying concentrations of a fluorescent tracer. Similar measurements could be made by tagging the molecule of interest with a fluorescent marker using this same experimental protocol. Alternatively, samples of interstitial fluid could be directly collected from the gel filling ports in the device, and used to quantify transport into the matrix, but this could be problematic due to the low drug concentrations in the gel region.

Although PDMS is widely used for microfluidic applications, one of its disadvantages is non-specific adsorption of proteins and small hydrophobic molecules during long-term interaction [67]. Even though this would not have affected our current permeability study, in perspective of drug testing, several treatments exist to prevent fouling of the PDMS surface. Accordingly, distinct surface modifications that could reduce non-specific absorption include coating the PDMS surface with bovine serum albumin (BSA) [68], grafting with anti-fouling molecules [69], or silanization [70].

Other possible improvements to the current model are the introduction of continuous perfusion to improve microvascular formation and reduce vascular permeability in the perspective of a long-term culture system. Indeed, flow perfusion culture could advance the model in two important aspects. Firstly, oxygen and glucose transport into the vessels will tend to modulate glycolytic metabolism in favor of the more efficient aerobic respiration useful for maintaining a long-term culture. Secondly, flow-mediated shear stress is known to promote the differentiation of vascular endothelial cells into a more BBB-like phenotype with the highest expression of TJ proteins and membrane transporters, producing further reductions in permeability [71]. Finally, it would be beneficial to assess the trans-endothelial electrical resistance (TEER) measurement as another metric of BBB function [24].

Conclusion

Here we present the first highly functional 3D BBB *in vitro* model produced by vasculogenesis that incorporate human iPSC-ECs microvascular network in contact interaction with human brain PCs and ACs within a single 3D ECM/fibrin gel region. Our 3D BBB microvascular model exhibits physiologically relevant structures and provides an effective and reproducible platform compared to static models [16][17], useful in the study of dynamic transport of small and large molecules across the BBB in a complex microenvironment [72]. We believe this is a reliable and valuable next-generation system that furthers the understanding of neurovascular function, enables the preclinical development of effective CNS therapeutics [16], can be applied to probe metastatic cancer extravasation [26][73] and evaluate reciprocal brain-systemic circulation interactions that occur in inflammatory and neurodegenerative diseases [4-9]. This translational model could be adapted for the high-throughput pre-clinical screening of innovative therapies targeting specific BBB transporters, to perform drug delivery studies and to investigate the transport of microengineered nanocarriers able to cross the BBB.

References

[1] N. J. Abbott, “Dynamics of CNS barriers: Evolution, differentiation, and modulation,” *Cell. Mol. Neurobiol.*, vol. 25, no. 1, pp. 5–23, 2005.

[2] N. J. Abbott, A. A. K. Patabendige, D. E. M. Dolman, S. R. Yusof, and D. J. Begley, “Structure and function of the blood-brain barrier,” *Neurobiol. Dis.*, vol. 37, no. 1, pp. 13–25, 2010.

[3] Y. Serlin, I. Shelef, B. Knyazer, and A. Friedman, “Anatomy and physiology of the blood-brain barrier,” *Semin. Cell Dev. Biol.*, vol. 38, pp. 2–6, 2015.

[4] R. D. B. B. V. Zlokovic, “Neurovascular mechanisms and blood–brain barrier disorder in Alzheimer’s disease,” *Acta Neuropathol.*, vol. 36, no. 3, pp. 490–499, 2010.

[5] B. V. Zlokovic, “Neurovascular mechanisms of Alzheimer’s neurodegeneration,” *Trends Neurosci.*, vol. 28, no. 4, pp. 202–208, 2005.

[6] R. Kortekaas *et al.*, “Blood-brain barrier dysfunction in Parkinsonian midbrain in vivo,” *Ann. Neurol.*, vol. 57, no. 2, pp. 176–179, 2005.

[7] E. Waubant, “Biomarkers indicative of blood-brain barrier disruption in multiple sclerosis.,” *Dis. Markers*, vol. 22, no. 4, pp. 235–244, 2006.

[8] R. K. Jain, E. Di Tomaso, D. G. Duda, J. S. Loeffler, A. G. Sorensen, and T. T. Batchelor, “Angiogenesis in brain tumours,” *Nat. Rev. Neurosci.*, vol. 8, no. 8, pp. 610–622, 2007.

[9] B. T. Hawkins and T. P. Davis, “The Blood-Brain Barrier / Neurovascular Unit in Health and Disease,” *Pharmacol. Rev.*, vol. 57, no. 2, pp. 173–185, 2005.

[10] W. M. Pardridge, “CSF, blood-brain barrier, and brain drug delivery.,” *Expert Opin. Drug Deliv.*, vol. 5247, no. May, pp. 1–13, 2016.

[11] W. M. Pardridge, “Why is the global CNS pharmaceutical market so under-penetrated?,” *Drug Discov. Today*, vol. 7, no. 1, pp. 5–7, 2002.

[12] W. M. Pardridge, “Blood-brain barrier drug targeting: the future of brain drug development.,” *Mol. Interv.*, vol. 3, no. 2, pp. 90–105, 51, 2003.

[13] N. J. Abbott, “Prediction of blood–brain barrier permeation in drug discovery from in vivo, in vitro and in silico models,” *Drug Discov. Today Technol.*, vol. 1, no. 4, pp. 407–416, Dec. 2004.

[14] D. Pamies, T. Hartung, and H. T. Hogberg, “Biological and medical applications of a brain-on-a-chip.,” *Exp. Biol. Med. (Maywood).*, pp. 1096–1107, 2014.

[15] P. S., “Preclinical research: Make mouse studies work,” *Nature*, vol. 507, no. 425, 2014.

[16] R. Cecchelli *et al.*, “Modelling of the blood–brain barrier in drug discovery and development,” *Nat. Rev. Drug Discov.*, vol. 6, no. 8, pp. 650–661, 2007.

[17] M. W. van der Helm, A. D. van der Meer, J. C. T. Eijkel, A. van den Berg, and L. I. Segerink, “Microfluidic organ-on-chip technology for blood-brain barrier research.,” *Tissue barriers*, vol. 4, no. 1, p. e1142493, 2016.

[18] K. Hatherell, P. O. Couraud, I. A. Romero, B. Weksler, and G. J. Pilkington, “Development of a three-dimensional, all-human in vitro model of the blood-brain barrier using mono-, co-, and tri-cultivation Transwell models,” *J. Neurosci. Methods*, vol. 199, no. 2, pp. 223–229, 2011.

[19] N. J. Abbott, L. Rönnbäck, and E. Hansson, “Astrocyte-endothelial interactions at the blood-brain barrier,” *Nat. Rev. Neurosci.*, vol. 7, no. 1, pp. 41–53, 2006.

[20] M. D. Sweeney, S. Ayyadurai, and B. V Zlokovic, “Pericytes of the neurovascular unit: key functions and signaling pathways,” *Nat. Neurosci.*, vol. 19, no. 6, pp. 771–783, 2016.

[21] C. F. Cho *et al.*, “Blood-brain-barrier spheroids as an in vitro screening platform for brain-penetrating agents,” *Nat. Commun.*, vol. 8, pp. 1–14, 2017.

[22] E. Urich, C. Patsch, S. Aigner, M. Graf, R. Iacone, and P. O. Freskgård, “Multicellular self-assembled spheroidal model of the blood brain barrier,” *Sci. Rep.*, vol. 3, 2013.

[23] J. D. Wang, E. S. Khafagy, K. Khanafer, S. Takayama, and M. E. H. Elsayed, “Organization of Endothelial Cells, Pericytes, and Astrocytes into a 3D Microfluidic in Vitro Model of the Blood-Brain Barrier,” *Mol. Pharm.*, vol. 13, no. 3, pp. 895–906, 2016.

[24] R. Booth and H. Kim, “Characterization of a microfluidic in vitro model of the blood-brain barrier (μBBB),” *Lab Chip*, vol. 12, no. 10, p. 1784, 2012.

[25] H. Cho *et al.*, “Three-Dimensional Blood-Brain Barrier Model for in vitro Studies of Neurovascular Pathology,” *Sci. Rep.*, vol. 5, p. 15222, 2015.

[26] H. Xu *et al.*, “A dynamic in vivo-like organotypic blood-brain barrier model to probe metastatic brain tumors,” *Sci. Rep.*, vol. 6, no. 1, p. 36670, 2016.

[27] A. Herland, A. D. van der Meer, E. A. FitzGerald, T.-E. Park, J. J. F. Sleeboom, and D. E. Ingber, “Distinct Contributions of Astrocytes and Pericytes to Neuroinflammation Identified in a 3D Human Blood-Brain Barrier on a Chip,” *PLoS One*, vol. 11, no. 3, p. e0150360, 2016.

[28] I. M. Braverman, “The Cutaneous Microcirculation,” *J. Investig. Dermatology Symp. Proc.*, vol. 5, no. 1, pp. 3–9, 2000.

[29] A. D. Wong, M. Ye, A. F. Levy, J. D. Rothstein, D. E. Bergles, and P. C. Searson, “The blood-brain barrier: an engineering perspective,” *Front. Neuroeng.*, vol. 6, no. August, pp. 1–22, 2013.

[30] T. Takano *et al.*, “Astrocyte-mediated control of cerebral blood flow.,” *Nat. Neurosci.*, vol. 9, no. 2, pp. 260–267, 2006.

[31] K. Kisler, A. R. Nelson, A. Montagne, and B. V. Zlokovic, “Cerebral blood flow regulation and neurovascular dysfunction in Alzheimer disease,” *Nat. Rev. Neurosci.*, vol. 18, no. 7, pp. 419–434, 2017.

[32] G. Adriani, D. Ma, A. Pavesi, and R. D. Kamm, “A 3D neurovascular microfluidic model consisting of neurons, astrocytes and cerebral endothelial cells as a blood–brain barrier,” *Lab Chip*, vol. 12, pp. 169–182, 2017.

[33] J. A. Whisler, M. B. Chen, and R. D. Kamm, “Control of perfusable microvascular network

morphology using a multiculture microfluidic system.," *Tissue Eng. Part C. Methods*, vol. 20, no. 7, pp. 543–52, 2014.

[34] S. Bang *et al.*, "A Low Permeability Microfluidic Blood-Brain Barrier Platform with Direct Contact between Perfusable Vascular Network and Astrocytes," *Sci. Rep.*, vol. 7, no. 1, p. 8083, 2017.

[35] E. a Winkler, R. D. Bell, and B. V Zlokovic, "Central nervous system pericytes in health and disease.," *Nat. Neurosci.*, vol. 14, no. 11, pp. 1398–1405, 2011.

[36] Y. Shin *et al.*, "Reconstituting vascular microenvironment of neural stem cell niche in three-dimensional extracellular matrix," *Adv. Healthc. Mater.*, vol. 3, no. 9, pp. 1457–1464, 2014.

[37] Y. Shin *et al.*, "Microfluidic assay for simultaneous culture of multiple cell types on surfaces or within hydrogels," *Nat. Protoc.*, vol. 7, no. 7, pp. 1247–1259, 2012.

[38] A. Hasan *et al.*, "Microfluidic techniques for development of 3D vascularized tissue," *Biomaterials*, vol. 35, no. 26, pp. 7308–7325, 2014.

[39] K. Haase and R. D. Kamm, "Advances in on-chip vascularization.," *Regen. Med.*, vol. 12, no. 3, pp. 285–302, 2017.

[40] F. E. Curry, V. H. Huxley, and R. H. Adamson, "Permeability of single capillaries to intermediate-sized colored solutes.," *Am. J. Physiol.*, vol. 245, no. 3, pp. H495-505, 1983.

[41] D. G. Belair *et al.*, "Human vascular tissue models formed from human induced pluripotent stem cell derived endothelial cells," *Stem Cell Rev. Reports*, vol. 11, no. 3, pp. 511–525, 2015.

[42] S. Kim, H. Lee, M. Chung, and N. L. Jeon, "Engineering of functional, perfusable 3D microvascular networks on a chip," *Lab Chip*, vol. 13, no. 8, pp. 1489–1500, 2013.

[43] and R. D. K. Michelle B. Chen, Jordan A. Whisler , Jessie S. Jeon, "Mechanisms of tumor cell extravasation in an in vitro microvascular network platform," *Integr. Biol.*, vol. 144, no. 5, pp. 724–732, 2014.

[44] J. S. Jeon *et al.*, "Generation of 3D functional microvascular networks with human mesenchymal stem cells in microfluidic systems," *Integr. Biol.*, vol. 6, no. 5, pp. 555–563, 2014.

[45] T. Osaki, Y. Shin, V. Sivathanu, M. Campisi, and R. D. Kamm, "In Vitro Microfluidic Models for Neurodegenerative Disorders," *Adv. Healthc. Mater.*, vol. 1700489, p. 1700489, 2017.

[46] P. Kreczmanski *et al.*, "Microvessel length density, total length, and length per neuron in five subcortical regions in schizophrenia," *Acta Neuropathol.*, vol. 117, no. 4, pp. 409–421, 2009.

[47] B. Obermeier, R. Daneman, and R. M. Ransohoff, "Development, maintenance and disruption of the blood-brain-barrier," *Nat. Med.*, vol. 19, no. 12, pp. 1584–1596, 2013.

[48] N. Hagan and A. Ben-Zvi, "The molecular, cellular, and morphological components of blood-brain barrier development during embryogenesis," *Semin. Cell Dev. Biol.*, vol. 38, pp. 7–15, 2015.

[49] R. Daneman, L. Zhou, A. A. Kebede, and B. A. Barres, "Pericytes are required for blood-brain barrier integrity during embryogenesis," *Nature*, vol. 468, no. 7323, pp. 562–566, 2010.

[50] G. Bergers and S. Song, "The role of pericytes in blood-vessel formation and maintenance.," *Neuro.*

759 *Oncol.*, vol. 7, no. 4, pp. 452–464, 2005.
760 [51] M. A. Proescholdt *et al.*, “Vascular endothelial growth factor (VEGF) modulates vascular
761 permeability and inflammation in rat brain.,” *J. Neuropathol. Exp. Neurol.*, 1999.
762 [52] J. Kim, M. Chung, S. Kim, D. H. Jo, J. H. Kim, and N. L. Jeon, “Engineering of a biomimetic
763 pericyte-covered 3D microvascular network,” *PLoS One*, vol. 10, no. 7, pp. 1–15, 2015.
764 [53] R. C. Brown, A. P. Morris, and R. G. O’Neil, “Tight junction protein expression and barrier
765 properties of immortalized mouse brain microvessel endothelial cells,” *Brain Res.*, vol. 1130, no. 1,
766 pp. 17–30, 2007.
767 [54] M. D. Sweeney, S. Ayyadurai, and B. V Zlokovic, “Pericytes of the neurovascular unit: key functions
768 and signaling pathways.,” *Nat. Neurosci.*, vol. 19, no. 6, pp. 771–83, 2016.
769 [55] B. Prabhakarpandian *et al.*, “SyM-BBB: a microfluidic Blood Brain Barrier model,” *Lab Chip*, vol.
770 13, no. 6, pp. 1093–1101, 2013.
771 [56] W. Löscher and H. Potschka, “Blood-brain barrier active efflux transporters: ATP-binding cassette
772 gene family,” *NeuroRX*, vol. 2, no. 1, pp. 86–98, 2005.
773 [57] S. Banerjee and M. A. Bhat, “Neuron-Glial Interactions in Blood-Brain Barrier Formation,” *Annu.
774 Rev. Neurosci.*, vol. 30, pp. 235–258, 2007.
775 [58] S.-W. Lee *et al.*, “SSeCKS regulates angiogenesis and tight junction formation in blood-brain
776 barrier.,” *Nat. Med.*, vol. 9, no. 7, pp. 900–906, 2003.
777 [59] D. J. Begley, “Delivery of therapeutic agents to the central nervous system: the problems and the
778 possibilities.,” *Pharmacol. Ther.*, vol. 104, no. 1, pp. 29–45, 2004.
779 [60] W. Yuan, Y. Lv, M. Zeng, and B. M. Fu, “Non-invasive measurement of solute permeability in
780 cerebral microvessels of the rat,” *Microvasc. Res.*, vol. 77, no. 2, pp. 166–173, Mar. 2009.
781 [61] S. Y. Shi L., Zeng M., “Quantification of Blood-Brain Barrier Solute Permeability and Brain
782 Transport by Multiphoton Microscopy,” vol. 136, no. March 2014, pp. 1–9, 2014.
783 [62] Y. I. Wang, H. E. Abaci, and M. L. Shuler, “Microfluidic blood-brain barrier model provides in vivo-
784 like barrier properties for drug permeability screening,” *Biotechnol. Bioeng.*, vol. 114, no. 1, pp. 184–
785 194, 2017.
786 [63] S. G. Canfield *et al.*, “An isogenic blood-brain model comprising brain endothelial cells, astrocytes
787 and neurons derived from human induced pluripotent stem cells,” *Neurochem. J. O F*, no. 140, pp.
788 874–888, 2017.
789 [64] J. M. Guanglei Li, Melissa J. Simon, Limary M. Cancel, Zhong-Dong Shi, Xinying Ji and and B. M.
790 F. Tarbell, Barclay Morrison, “Permeability of Endothelial and Astrocyte Cocultures: In Vitro Blood–
791 Brain Barrier Models for Drug Delivery Studies,” *Annu. Biomed. Eng.*, vol. 38, no. 8, pp. 2499–2511,
792 2010.
793 [65] J. D. Huber, K. A. Witt, S. Hom, R. D. Egleton, K. S. Mark, and T. P. Davis, “Inflammatory pain
794 alters blood-brain barrier permeability and tight junctional protein expression.,” *Am. J. Physiol. Heart*

Circ. Physiol., vol. 280, no. 3, pp. H1241–H1248, 2001.

[66] A. Appelt-Menzel *et al.*, "Establishment of a Human Blood-Brain Barrier Co-culture Model Mimicking the Neurovascular Unit Using Induced Pluri- and Multipotent Stem Cells," *Stem Cell Reports*, vol. 8, no. 4, pp. 894–906, 2017.

[67] M. W. Toepke and D. J. Beebe, "PDMS absorption of small molecules and consequences in microfluidic applications," *Lab Chip*, no. c, pp. 1484–1486, 2006.

[68] E. Ostuni, C. S. Chen, D. E. Ingber, and G. M. Whitesides, "Selective Deposition of Proteins and Cells in Arrays of Microwells," *Langmuir*, vol. 17, no. 9, pp. 2828–2834, 2001.

[69] A. Gokaltun, M. L. Yarmush, A. Asatekin, and O. B. Usta, "Recent advances in nonbiofouling PDMS surface modification strategies applicable to microfluidic technology," *Technology*, vol. 5, no. 1, pp. 1–12, 2017.

[70] S. Jon, J. Seong, A. Khademhosseini, T. T. Tran, P. E. Laibinis, and R. Langer, "Construction of Nonbiofouling Surface by Polymeric Self-Assembled Monolayers," *Langmuir*, vol. 19, no. 24, pp. 0–4, 2003.

[71] L. Cucullo, M. Hossain, V. Puvenna, N. Marchi, and D. Janigro, "The role of shear stress in Blood-Brain Barrier endothelial physiology," *BMC Neurosci.*, vol. 12, no. 1, p. 40, 2011.

[72] C. Hajal *et al.*, "In vitro models of molecular and nano-particle transport across the blood-brain barrier In vitro models of molecular and nano-particle transport across the blood-brain barrier," *Biomicrofluidics*, vol. 42213, no. 12, 2018.

[73] M. B. Chen, J. A. Whisler, J. Fröse, C. Yu, Y. Shin, and R. D. Kamm, "On-chip human microvasculature assay for visualization and quantification of tumor cell extravasation dynamics," *Nat. Protoc.*, vol. 12, no. 5, pp. 865–880, 2017.

Acknowledgements

M.C. was supported by Ermenegildo Zegna Founder's scholarship and then by the MIT-POLITO grant (BIOMODE - Compagnia di San Paolo) under the joint "Doctorate of Bioengineering and Medical-Surgical Sciences" of University of Turin and Politecnico di Torino. Y.S. and R.K. were supported by grants from the Cure Alzheimer's Fund. T.O. was supported by research fellow overseas (Japan Society for the Promotion of Science). R.K. and T.O also acknowledge the support of National Science Foundation for a Science and Technology Center on Emergent Behaviors of Integrated Cellular Systems, (CBET-0939511). C.H. and R.K. were supported by the National Cancer Institute (U01 CA202177). M.C., V.C., and R.K. also acknowledge the support of the research collaborations and exchanges program between MIT and POLITO (MITOR project NANOCAB).

Author contributions

All authors designed the experiments. M.C. performed majority of experiments, analyzed all data, and wrote the manuscript. Y.S designed the microfluidic device and highly contributed to perform immunocytochemistry, permeability assays and vascular parameters analysis. T.O. designed and contributed to RT-PCR experiments, schematic drawings of this paper, statistical tests, discussion and writing of the manuscript. C.H. and M.C. performed vascular parameters analysis. R.K. and V.C. co-supervised the project. V.C. provided inputs in the writing of the manuscript. R.K. provided critical inputs to the experimental design and writing of the manuscript. All authors reviewed and accepted the manuscript.

Additional information

Competing financial interests

R.K. is co-founder and has a significant financial interest in AIM Biotech, a company that manufactures microfluidic systems.